Online analysis of oxygen inside silicon-glass microreactors with integrated optical sensors

Ehgartner, Josef; Sulzer, Philipp; Burger, Tobias; Kasjanow, Alice; Bouwes, Dominique; Krühne, Ulrich; Klimant, Ingo; Mayr, Torsten

Published in:
Sensors and Actuators B: Chemical

Link to article, DOI:
10.1016/j.snb.2016.01.050

Publication date:
2016

Document Version
Publisher's PDF, also known as Version of record

Sensors and Actuators B 228 (2016) 748–757

Contents lists available at ScienceDirect

Sensors and Actuators B: Chemical

journal homepage: www.elsevier.com/locate/snb

Online analysis of oxygen inside silicon-glass microreactors with integrated optical sensors

Josef Ehgartner[a], Philipp Sulzer[a], Tobias Burger[a], Alice Kasjanow[b], Dominique Bouwes[b], Ulrich Krühne[c], Ingo Klimant[a], Torsten Mayr[a,*]

[a] Institute of Analytical Chemistry and Food Chemistry, Graz University of Technology, Stremayrgasse 9/3, 8010 Graz, Austria
[b] iX-factory GmbH, 44263 Dortmund, Germany
[c] Centre for Process Engineering and Technology, Department of Chemical and Biochemical Engineering, Technical University of Denmark, Søltofts plads, 2800 Kgs. Lyngby, Denmark

ARTICLE INFO

Article history:
Received 30 September 2015
Received in revised form 7 January 2016
Accepted 13 January 2016
Available online 19 January 2016

Keywords:
Optical oxygen sensor
Microfluidics
Microreactor
Integrated sensor
Enzyme reactions

ABSTRACT

A powerful online analysis set-up for oxygen measurements within microfluidic devices is presented. It features integration of optical oxygen sensors into microreactors, which enables contactless, accurate and inexpensive readout using commercially available oxygen meters via luminescent lifetime measurements in the frequency domain (phase shifts). The fabrication and patterning of sensor layers down to a size of 100 μm in diameter is performed via automated airbrush spraying and was used for the integration into silicon-glass microreactors. A novel and easily processable sensor material is also presented and consists of a polystyrene- silicone rubber composite matrix with embedded palladium(II) or platinum(II) *meso*-tetra(4-fluorophenyl) tetrabenzoporphyrin (PdTPTBPF and PtTPTBPF) as oxygen sensitive dye. The resulting sensor layers have several advantages such as being excitable with red light, emitting in the near-infrared spectral region, being photostable and covering a wide oxygen concentration range. The trace oxygen sensor (PdTPTBPF) in particular shows a resolution of 0.06–0.22 hPa at oxygen concentrations lower than 20 hPa (< 2% oxygen) and the normal range oxygen sensor (PtTPTBPF) shows a resolution of 0.2–0.6 hPa at low oxygen concentrations (< 50 hPa) and 1–2 hPa at ambient air oxygen concentrations. The sensors were integrated into different silicon-glass microreactors which were manufactured using mass production compatible processes. The obtained microreactors were applied for online monitoring of enzyme transformations, including D-alanine or D-phenylalanine oxidation by D-amino acid oxidase, and glucose oxidation by glucose oxidase.

1. Introduction

Microfluidic platforms are useful tools for studying organic reactions [1], enzyme kinetics [2–4] and cells [5–8] at micro- or nanoscale. The small volumes of such devices allow a view behind the scenes of bulk characteristics of molecules, enzymes and cells. Faced with decreasing dimensions, however, analytical chemists are challenged to find new methods to determine analytes accurately. The integration of luminescent chemical sensors into microfluidic devices can be one useful technique for obtaining online and real-time analytical data at this miniaturized scale [9,10]. Luminescent oxygen sensors are highly suited for microfluidic applications due to their high sensitivity, ability of contactless readout, ease of miniaturization, ease of integration and their low cost [11]. Moreover, optical oxygen sensors do not need a reference element and do not deplete oxygen during the measurement in comparison to electrochemical sensors. Nonetheless, ground state triplet oxygen is transformed into reactive excited state singlet oxygen during the quenching process of the luminescent oxygen sensors [12–14]. The excited state singlet oxygen can react with its surrounding environment and therefore can bias the investigated system in the microscale [15].

One of the first publications dealing with the integration of a luminescent oxygen sensor into a silicon based microfluidic device was from Sin et al [16]. They developed a cell culture system for mammalian cells and machined a 3 mm × 3 mm × 0.15 mm recess into the bottom plate of the chip which was filled with a resin-adsorbed ruthenium(II) complex as oxygen indicator dye and poly(dimethylsiloxane) (PDMS) to obtain an oxygen sensor patch. The oxygen sensor was chosen as a proof-of-concept inte-

* Corresponding author.
E-mail address: torsten.mayr@tugraz.at (T. Mayr).

http://dx.doi.org/10.1016/j.snb.2016.01.050

grated sensor and used to monitor the adequate oxygen supply for the cells. In another study Thorsen et al. [17,18]. showed the integration of a sensor layer consisting of platinum(II) octaethylporphyrin-ketone and polystyrene into a PDMS-based microfluidic differential oxygenator for cell culture. A sensor solution was manually pipetted onto etched glass slides, the solvent was evaporated and the functionalized glass slide was bonded by an oxygen plasma treatment to a structured PDMS layer. The same sensor chemistry was used by Nock et al [19,20]. to integrate a patterned sensor film within a PDMS-based microfluidic device. The patterning process included spin-coating of the sensor film onto a glass slide and patterning either by soft-lithography with PDMS stamps and reactive ion etching in an oxygen plasma [19] or a process based on a sacrificial metal layer and plasma patterning of the spin-coated sensor layer [20]. Etzkorn et al. fabricated oxygen sensor rings on glass wafers by spin coating in combination with a photopatterning process [21]. The sensors were used to determine the oxygen consumption rates of single cells in glass microwell arrays. Another study introduced oxygen sensor beads in microwells. The adherence of the sensor beads to the glass well was achieved by slightly melting them [22]. Commercially available oxygen sensor patches were also integrated into microbioreactors for monitoring oxygen during microbial fermentations [23–25]. In other studies prefabricated spin coated sensor layers containing a platinum(II)-porphyrin complex were used in microfluidic devices for regulating oxygen levels [26,27] and for cell culture [28]. In another study a similar sensor chemistry was integrated into microfluidic channels of a PDMS-glass-based microscale reactor [29]. The oxygen sensor was spin-coated onto a glass substrate which already contained microchannels. The sensing layer outside of the microchannels was removed with a razor blade, prior to assemble the microscale reactor. Grist et al. used a laser cutter system to pattern oxygen sensing films [30]. Spin-coated polystyrene films were structured by the laser cutter and the unwanted bulk film was removed by aqueous lift-off/peeling. In another study, we reported recently the introduction of oxygen-sensitive conjugated polymer nanoparticles into microfluidic devices [31]. As described above, integration and patterning of oxygen sensor layers into microfluidic devices were often accomplished by spin coating of a sensor solution onto a substrate in combination with the removal of the surplus bulk material. In further reports optical chemical sensors for other analytes like pH were also incorporated by inkjet printers into microfluidic devices [32–35]. Herein, we demonstrate that airbrush spraying in combination with stencils is a promising alternative to incorporate patterned oxygen sensing layers into microfluidic devices. Moreover, we adapted commercially available oxygen meters to make them ready for use in microfluidic applications. The presented oxygen sensor layers are an improvement to former reports because they show a higher brightness (BS = $\varepsilon \times$ quantum yield), are excitable with red light, emit in the near infrared (a spectral region where fewer compounds emit) and are fully compatible with the used oxygen meters [36]. Furthermore, we tested our set-up in silicon-glass microreactors for online monitoring of oxygen by different oxygen depleting enzyme reactions.

2. Experimental

2.1. Materials

Palladium(II) and platinum(II) *meso*-tetra(4-fluorophenyl) tetrabenzoporphyrin (PdTPTBPF and PtTPTBPF, respectively; chemical structures supplementary Fig. S.1) were synthesized in-house according to the literature procedure [37]. Polystyrene (PS; average molecular weight = 250 000 g/mol) was purchased from Fisher Scientific (www.fishersci.com), chloroform and D(+)-glucose monohydrate were bought from Roth (www.carl-roth.de). Silicone rubber ELASTOIL® E4 was obtained from Wacker (www.wacker.com). D-phenylalanine, D-alanine, D-amino acid oxidase from porcine kidney, glucose oxidase from *Aspergillus niger*, catalase from bovine liver and poly(ethylene glycol) (PEG 6000, av. MW = 6000) were purchased from Sigma–Aldrich, gases for calibration from Linde (www.linde-gas.at). Photoresists ma-P 1240 and mr-D 526 were obtained from micro resist technology (www.microresist.de).

The microreactors were manufactured using batch-production compatible processes. The general steps of the production process are described below (Fig. 1). The designed microreactors consist of a silicon part with microfluidic structures and a glass part with integrated oxygen sensors and access holes. Silicon wafers were structured by a photolithography process followed by dry etching. The use of silicon together with dry etching allowed the production of microfluidic structures with aspect ratios up to 1:20 and a nearly perpendicular channel-profile, which is not possible with glass.

A silicon wafer (crystal orientation = 100) with a thickness of 675 μm was coated with a positive photoresist (ma-P 1240). The photoresist had a layer thickness of 4 μm and was baked for 2 min at 95 °C. This photoresist is highly stable in dry etching processes. An UV-lithography was performed with a mask aligner from Suss Microtec (www.suss.com) with a dose of 110 mJ/cm^2. Alignment marks in the channel design will guarantee an accurate positioning of the access holes in the glass wafer. After developing for 2 min in a beaker with mr-D 526 developer the wafer was rinsed with deionized water for 2 min. The Bosch process was applied for the etching to reach a channel depth of 200 μm. The etching was performed in a deep reactive ion etcher (Alcatel AMS 110). The etch gasses SF_6/C_4F_8 (400/200 sccm) were alternately introduced for 2.5 s at a power of 2000 W in a capacitive coupled plasma of 50 W. After etching the wafer, the resist was removed in an oxygen plasma. The resist stripping was done in a plasma etcher from PVA TePla (www.pvatepla.com) with 200 sccm oxygen at 500 W for 15 min. The depth was measured with a profiler. In parallel, a stencil mask for the sensor areas was fabricated. A silicon wafer (crystal orientation = 100) with a thickness of 300 μm was coated with the positive photo-resist (ma-P 1240) and processed as described above. During the dry etching, trenches were etched, which were the openings for the spray-coating procedure (described below). Before the stencil mask was used, the fluidic access holes were fabricated into the glass wafer. Therefore either powder blasting or laser drilling can be applied. A photolithography process was required as described above for powder blasting. The holes have a diameter of 1.5 mm. Subsequently, the stencil mask was positioned on the alignment marks on top of the glass wafer and fixed with tape (Kapton® or UV removable tape). In the next step, the sensing areas were spray-coated as described below. After integration of the sensing area, the tape can be easily removed and the stencil mask can be reused for the next spraying process. The silicon wafer and the glass wafer were anodic bonded using a CB8 wafer bonder from Suss Microtec. During this process step, the microfluidic channels were closed. To secure the functionality of the sensors, the bond temperature was decreased to 180 °C but the bonding time had to be increased. The anodic bonding was realized at 1000 V and a pressure of 5 kN within 4 h. The wafers were diced after bonding into microreactor chips in the size of microscopic slides (75.5 mm × 25.5 mm) to achieve compatibility of the microfluidic modules with standard laboratory equipment. A DAD3350 dicing tool from Disco (www.discoeurope.com) with a dicing blade of 300 μm was used.

2.2. Integration and characterization of the oxygen sensors

Sensor dye (PdTPTBPF or PtTPTBPF; 0.45 mg), silicone rubber (30 mg) and polystyrene (15 mg) were dissolved in chloroform

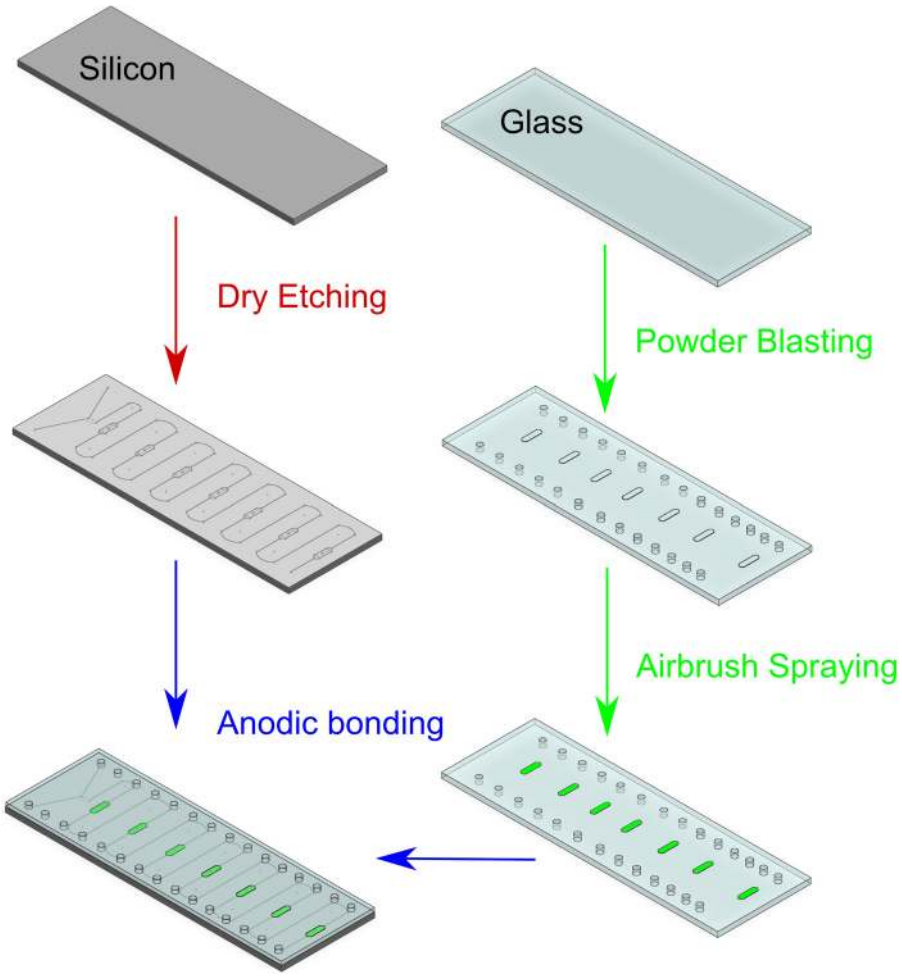

Fig. 1. Schematic overview of the chip-manufacturing process.

(1.5 g) to obtain a sensor "cocktail". Silicone rubber was added because of its better adherence properties for glass compared to polystyrene. This "cocktail" was deposited onto glass wafers with photomasks as stencils using an in-house developed computerized numerical control (CNC) air-brush spraying device (Supplementary Fig. S.2). The spraying device consists of an airbrush (EFBE Spritzautomat 1/2L, 0.2 mm nozzle diameter, www.efbe-airbrush.de) fixed to an *x*–*y*–*z* table actuated by stepper motors (two-phase-stepper-motor, www.isel-gmbh.com). The motors are controlled by a Triple Beast Driver (www.benezan-electronics.de), which also drives a fourth axis extension for the airbrush needle valve and a solenoid valve (SMC) for airflow switching. The opening of the airbrush needle valve in combination with the opening time determines the amount of deposited material. The spraying procedure was automated by using G-Code and LinuxCNC (www.linuxcnc.org). The sensor films were cured at 60 °C for 24 h. Layer thicknesses were determined on a Bruker DekTak XT surface profiler. After curing, the sensor layers were gas-phase calibrated in an in-house developed temperature controlled calibration chamber. Two mass flow controller instruments (Read Y smart series) by Vögtlin instruments (www.voegtlin.com) were used to obtain gas mixtures of defined oxygen partial pressures (pO_2). Compressed air, 2% (v/v) oxygen in nitrogen and nitrogen were used as calibration gases. The calibration gas was passed through a stainless steel coil which was dipped into a temperature-controlled water bath before reaching the calibration chamber. The sensor layers were calibrated again after the bonding procedure to study its influence on the sensor material.

2.3. Online monitoring of enzyme reactions

Microreactors were connected via an in-house developed chip holder (Fig. 2 and Supplementary Fig. S.3) to syringe pumps (Cavro® Centris pumps from Tecan, www.tecan.com) which were operated by a specially written Lab VIEW program (www.ni.com/labview) we developed for this purpose. The oxidations of D-alanine and D-phenylalanine by D-amino acide oxidase, and glucose oxidation by glucose oxidase were used as model reactions. Therefore, D-alanine (35.4 mg, 100 mM), D-phenylalanine (65.6 mg, 100 mM) and D-amino acid oxidase (2.1 mg) were thus each dissolved in 4 mL of 100 mM TRIS buffer, pH 8.3 containing PEG 6000 (50 mg). α-D(+)-glucose monohydrate (500 mg, 50 mM) and glucose oxidase (2.5 mg for the enzyme cascade with catalase, otherwise 0.9 mg) were dissolved each in 50 mL of 10 mM phosphate buffer, pH 7.0 containing sodium chloride (130 mM) and PEG 6000 (600 mg). The oxidation of glucose was carried out in the absence or presence of catalase (approx. 4 mg in 50 mL of 10 mM phosphate buffer containing 130 mM NaCl and 600 mg PEG 6000). A two point calibration of the oxygen sensors was performed with air saturated water and deoxygenated water before the analysis. The microreactors were also purged with buffer containing 1% w/w PEG 6000 prior to the measurement to minimize non-specific binding of the enzymes to the surface. The microreactor contained two main inlets each connected to a separate syringe pump. One inlet was used to introduce the enzyme solution into the chip and the other to introduce the substrates. The catalase solution was introduced over a lateral inlet by a third syringe pump. The channels of the used

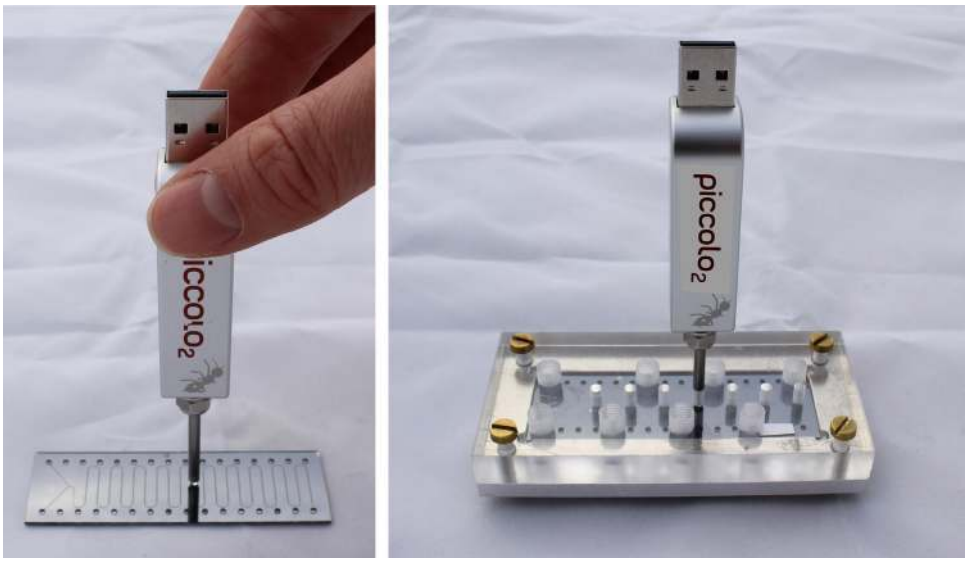

Fig. 2. Measurement set-up consisting of the USB oxygen meter, the microfluidic chip and the in-house developed chip holder.

microreactor were 200 μm or 400 μm deep and 100 μm or 200 μm wide. The flow rate during the oxidation of the amino acids was 0.6 μL/s (0.3 μL/s for each pump). Different flow rates (1.2 μL/s, 0.8 μL/s, 0.4 μL/s, 0.2 μL/s) were applied for the oxidation of glucose. All syringe pumps were operated at a flow rate of 0.1 μL/s for the catalase experiment. All enzyme reactions were carried out at room temperature. The oxygen measurements within the microreactor were carried out either with a 4-channel optical oxygen meter (FireStingO2) connected to optical fibres (Plastic fibre cable, simplex fibre 1 mm, PE-jacket 2.2 mm, www.ratioplast.com) or with a USB oxygen meter (Piccolo2) connected to a stainless steel tube including an optical plastic fibre (2 mm in diameter); both devices were obtained from Pyroscience (www.pyro-science.com). The optical fibre for the USB oxygen meter was adapted with a GRadient INdex (GRIN lens, www.grintech.de) to enhance the signal intensities, especially for smaller sensor layers. The lens was attached in front of the fibre. The modulation frequency of the optical oxygen meter was set to 4000 Hz for PtTPTBPF and to 400 Hz for PdTPTBPF. The intensity of the LED varied according to the sensor size but was generally set ≤60% and the amplification of signal was typically set ≤400×.

3. Results and discussion

We aimed to develop an analysis set-up based on optical sensors for the quantitative determination of oxygen. The development involved the following steps: (i) integration of sensor structures into silicon-glass microreactors, (ii) characterization of sensors, (iii) modification of measurement devices, and (iv) testing of the set-up.

3.1. Integration and characterization of oxygen sensors

Airbrush spraying was used to produce sensor films with different shapes and sizes, because similar to inkjet printing, it allows selective deposition and patterning of optical sensors at various positions along a microfluidic chip. The smallest sensor spots sprayed with stencils had diameters of 100 μm (Fig. 3) and spots sprayed without stencils had diameters of 2 mm. We obtained homogeneous sensor layers and used on average 2 μL sensor cocktail per spot (2 mm in diameter). In principle, one third of this volume would also lead to sufficient sensor signals. The airbrush spraying set-up can be used with sensor "cocktails" containing volatile solvents and is not prone to clogging when the sensor solution is sufficiently diluted. Sensor solutions should contain less than 2% w/w of polystyrene (molecular weight = 250 000 g/mol) to reliably operate the spraying system if chloroform is used as solvent. In addition, the used CNC airbrush spraying set-up can be programmed which is a helpful step for obtaining reproducible sensor layers. The thickness of the produced films can be adjusted by the number of spraying repetitions or by adjusting the opening of the needle valve. Our produced sensor layers had on average a thickness of 2.2 ± 0.2 μm (n = 7, spraying repetitions = 20), but also sensor layers with a thickness of approx. 0.5 μm provide sufficient signals with the used sensor cocktail. We deposited the sensing layers onto glass. The sensor material consisted of a polystyrene-silicone rubber composite matrix with the oxygen indicator dye physically entrapped. The addition of silicone rubber increases the adherence to glass due to its increased hydrophilicity compared to a common polystyrene matrix. The composite material exhibits additionally similar sensing properties for oxygen compared to polystyrene. The calibration curves of the new composite material and common polystyrene matrices are comparable (Supplementary Fig. S.4). We thus assume that the indicator dye is mostly entrapped in the polystyrene domains of the composite due to the low solubility of our indicator dyes in silicones [38].

Stern–Volmer calibration curves of the new sensing material are shown in Fig. 4. The calibration curves were recorded in replicates (n = 3). The error bars in Fig. 4 (hardly noticeable) reflect the variation of a single sensor layer calibrated three times. The relative standard deviations (RSD) are <0.5%. Calibration curves of independently manufactured sensing layers combined in one calibration (n = 3 for PdTPTBPF and n = 8 PtTPTBPF) are shown in Supplementary Fig. S.5. Their relative standard deviations (RSD) are <5% and reflect the variation of the manufacturing process. A simple two point calibration procedure is typically sufficient to achieve high accuracy. The two-site model was used to fit the calibration data [39] (Eq. (1)).

$$\frac{I_0}{I} = \frac{\tau_0}{\tau} = \left(\frac{f_1}{1 + K_{SV,1} \times pO_2} + \frac{f_2}{1 + K_{SV,2} \times pO_2}\right)^{-1} \quad (1)$$

The ratio I_0/I in the model was replaced by τ_0/τ where τ is the lifetime of the oxygen indicator dye at a certain pO_2-value, therefore the two-site model has no physical significance. The lifetime τ_0 represents the lifetime under deoxygenated conditions, where the oxygen indicator is in its unquenched state. The lifetimes were calculated from the phase shift $\Delta\varphi$ recorded by the oxygen meter

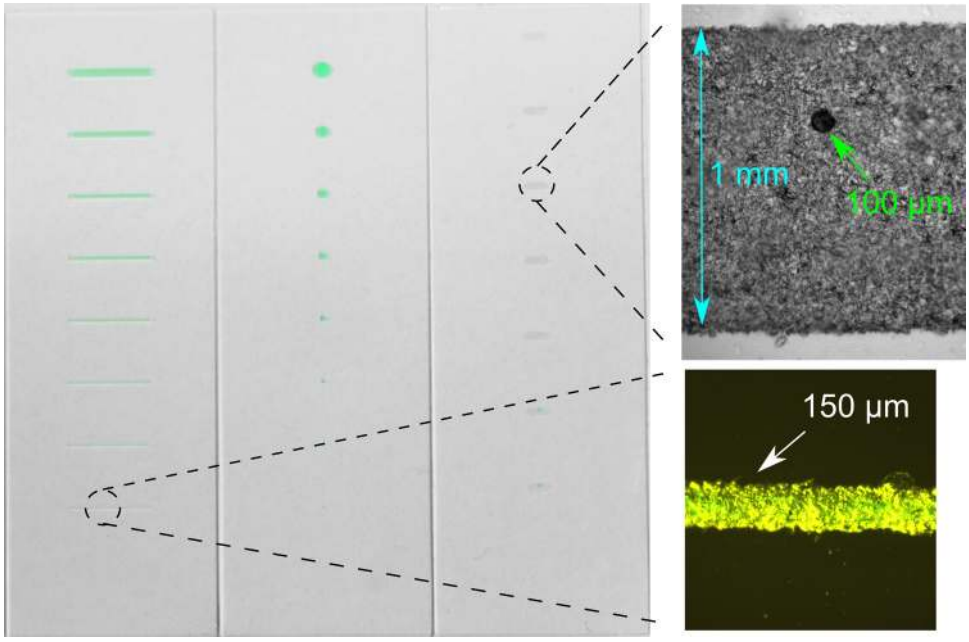

Fig. 3. Sensing lines or spots ranging from 1000 µm to 100 µm in width or diameter and microscopic bright-field images of a 100 µm sensor spot integrated into a 1 mm wide sensing area and of a 150 µm wide sensor line. Lines and spots were prepared by airbrush spraying in combination with stencils. Microscopic bright-field images were taken with a monochromatic camera (spot) or a color camera (line).

Table 1
Calibration parameters for the sensing layers at 20 °C.

	$K_{SV,1}$/* 10^{-3} hPa^{-1}	$K_{SV,2}$/* 10^{-3} hPa^{-1}	f_1
PtTPTBPF	17.4	2.03	0.821
PdTPTBPF	110.8	21.1	0.638

according to the equation $\tau = \tan(\Delta\varphi)/(2 \times \pi \times f)$, where f is the modulation frequency. The calibration parameters are shown in Table 1.

The resolution of the measurement set-up for the normal range oxygen sensor (PtTPTBPF) was about 0.2–0.6 hPa at low oxygen concentrations (<50 hPa) and about 1–2 hPa at ambient air oxygen concentrations (approx. 204 hPa at 980 mbar air pressure). The trace range oxygen sensor (<20 hPa; PdTPTBPF) showed a resolution of about 0.06–0.22 hPa. The resolution was calculated by inserting the upper and lower limit of a calibration point (mean value ± the standard deviation) into Eq. (1), the equation was solved for pO_2 and the difference was calculated out of these values. The limit of detection was 0.08 hPa for the normal range oxygen sensor and 0.009 hPa for the trace range oxygen sensor $[\tau_0/(\tau_0 \pm 3 \times \sigma)]$. Anodic bonding of the glass-silicon microreactors was performed at a temperature of approx. 180 °C and calibration before and after bonding revealed that the sensor materials became more sensitive after bonding (Supplementary Fig. S.5). We assume that the composite matrix became more permeable for oxygen due to the increased temperature during the bonding process. Nevertheless this does not have a significant impact on the sensor performance. In addition, the size of the sensing areas had no significant influence on the calibration function (Supplementary Figs. S.6 and S.7).

PdTPTBPF and PtTPTBPF were used because of their high brightness, excellent photostability and ideal spectral properties [36]. These dyes are excitable with red light, emit in the near infrared and therefore fulfil all the spectral requirements given by the used oxygen meters. Photostability tests of sensor spots (PtTPTBPF, 100 µm in diameter) revealed that illumination with a USB oxygen meter (Piccolo2) equipped with a focusing lens at maximum LED intensity resulted in no signal drift over more than 32 000 measurements points (corresponds to 9 h of continuous measurement at a measurement frequency of 1 measurement point per second, Supplementary Fig. S.8). Long-wavelength (above 600 nm) excitable and emissive indicators offer the advantage of less background fluorescence or scattering from polymer chips or biological matter (cells, proteins etc.). Moreover, excitation with red-light is less harmful to cells in comparison to UV or blue light.

3.2. Modification of measurement devices

The high brightness of the used dyes is beneficial for microfluidic applications because read out can be performed with standard optical fibres although the sensor areas are typically <1 mm^2. In addition, we modified a commercially available USB oxygen meter (Piccolo) with a gradient index lens to enhance the signal intensities by a factor of approx. 20 for smaller sensing areas (<0.05 mm^2). Furthermore, the Piccolo with the lens gave excellent signal-to-noise ratios of more than 500 for a sensor spot (200 µm in diameter) in close proximity (distance <0.5 mm, Supplementary Fig. S.11). This set-up thus offers the possibility of measuring even smaller sensor structures. Note that with decreasing sensor spot size the positioning of the measurement device requires more accurate and sophisticated set-ups. The advantage of the gradient index lens is that it focuses the excitation light exactly onto a sensing spot and thus enhances the signal intensities. The focused excitation light has approximately a diameter of 80 µm (Supplementary Fig. S.9). Further, we studied the influence of the distance between the measurement fibre and a sensor spot on the signal intensity (Supplementary Figs. S.10 and S.11). The distance between different fibres and sensor spots (200 µm or 1.4 mm in diameter) in water was adjusted by a *xyz*-micromanipulator and the signal intensities were recorded. Fibres with small diameters or fibres equipped with a lens provide high signal intensities at distances close to the sensor spot, but the collection of the emission light is less effective when the distances become longer. Hence, these systems are better suited for sensor spots which are in close proximity to the fibre/lens. The FireStingO2 oxygen meter offers the possibility that up to four sensor spots can be measured simultaneously compared

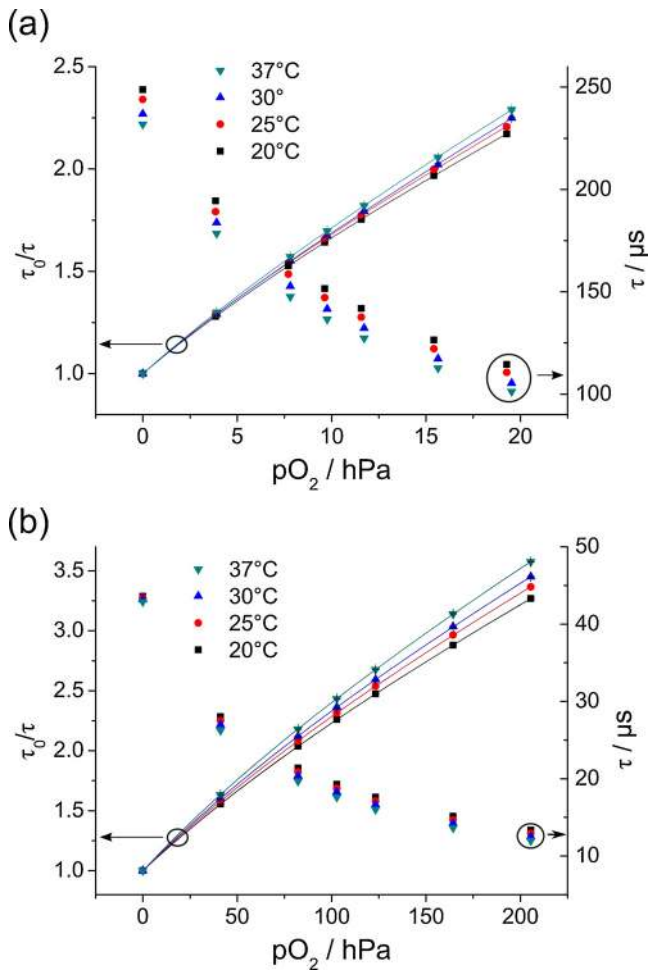

Fig. 4. Stern–Volmer calibration curves (left *Y*-axis) and luminescent lifetimes (right *Y*-axis) ($n = 3$ measurements) for the integrated trace range [PdTPTBPF, (a)] and normal range [PtTPTBPF, (b)] oxygen optodes at 20 °C, 25 °C, 30 °C and 37 °C. Lines indicate a fit according to Eq. (1).

to the Piccolo which scores with its smaller dimensions instead. In principle all of the used oxygen meters offer the advantage of being small, inexpensive and allowing accurate readout via luminescent lifetime measurements in the frequency domain, which is less prone to errors than intensity based methods. The benefit of luminescence lifetime measurements is that changes in the measurement conditions (alignment of the readout device, variations in the thickness of the sensor layer, variations of the intensity of the excitation light or of the incident light) do not result in significant signal changes compared to intensity measurements.

3.3. Online monitoring of enzyme reactions

The performance of the sensor- and measurement systems was tested in different glass-silicon microreactors (named *Microreactor 1–3)*. We used two model reactions to deplete the oxygen concentrations within the microreactors namely the oxidation of *beta*-D-glucose to D-glucono-1,5-lactone and hydrogen peroxide by glucose oxidase or the oxidation of D-amino acids to a 2-oxo carboxylate, ammonia and hydrogen peroxide by D-amino acid oxidase.

Microreactor 1 (channel dimensions: 200 μm deep, 100 μm wide; volume: 11.8 μL, Fig. 5) contained 7 chambers (dimensions: length 3.5 mm, width 1 mm). Each chamber contained a sensing spot (PtTPTBPF) with a diameter of either 100 μm, 200 μm or 300 μm. This demonstrates the miniaturization of the sensor

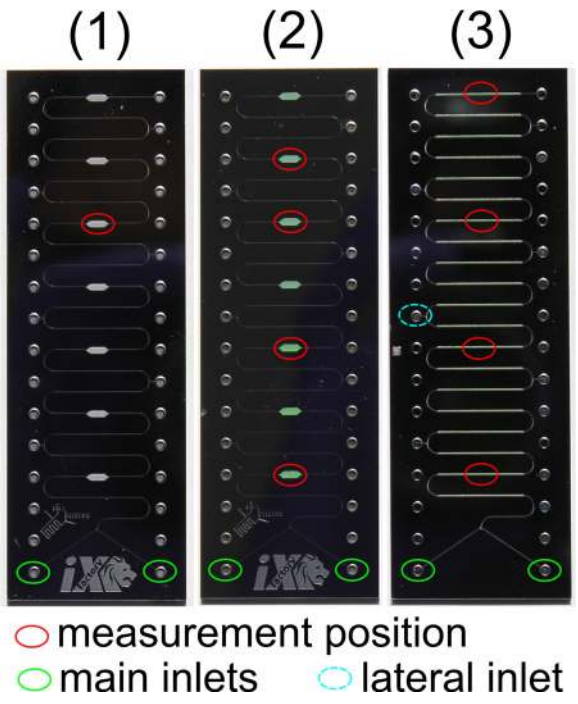

Fig. 5. Different types of microreactors. Microreactor (1) contained 7 chambers each containing a sensor spot with a diameter of 100 μm, 200 μm or 300 μm. In microreactor (2) the chambers were fully covered by oxygen sensors and microreactor (3) contained the oxygen sensor along the straight microfluidic structures of the channels.

areas. The response time (t_{90}) of these sensing set-ups to a rapid change in oxygen concentration from air saturation to anoxic conditions was approx. 3 s and determined by introducing gaseous nitrogen into the chip. The modified USB-oxygen meter was used as read out device to monitor the oxidation of glucose to D-glucono-δ-lactone and hydrogen peroxide by glucose oxidase at different flow rates [1.2 μL/s, 0.8 μL/s, 0.4 μL/s, 0.2 μL/s; Fig. 6(a)]. The measurement was performed at a 100 μm spot (in diameter) at the fifth chamber (counted from the inlets). The oxygen concentrations decreased within the microreactor with decreasing flow rate due to the longer residence time of the enzyme which is consuming the oxygen. Furthermore, the pumps stopped and refilled their syringes with either enzyme- or glucose solution before changing to a new flow rate. During this time (approx. 10–30 s) the glucose oxidase depleted the oxygen within the chamber which can be monitored online with our set-up [Fig. 6(a)]. Each flow rate was repeated three times and the oxygen concentrations were calculated out of the plateaus. The oxygen concentrations were 119.8 ± 0.7 hPa at 1.2 μL/s, 91.2 ± 0.5 hPa at 0.8 μL/s, 27.3 ± 0.5 hPa at 0.4 μL/s and < 0.6 hPa at 0.2 μL/s.

Microreactor 2 possessed the same characteristics (channel dimensions, response time, PtTPTBPF) as *microreactor 1* but the chambers were fully covered by the oxygen sensor. These sensor chambers allow an easier alignment of the read out system and exhibit higher signal intensities. Hence the read out could be performed by optical fibres (1 mm in diameter) connected to the 4-channel oxygen meter (FirestingO2). The set-up was used for online monitoring of the oxidation of D-alanine and D-phenylalanine by D-amino acid oxidase [Fig. 6(b) and (c)]. The oxygen depletion was simultaneously determined at four sensing spots which were chosen randomly. The microreactor was first flushed with water and then D-alanine and D-amino acid oxidase were introduced over two separate inlets at a flow rate of 0.6 μL/s (0.3 μL/s per pump). The pumps had to be refilled every 5.6 min indicated by the oxygen depletion within the microreactor due to the consumption of

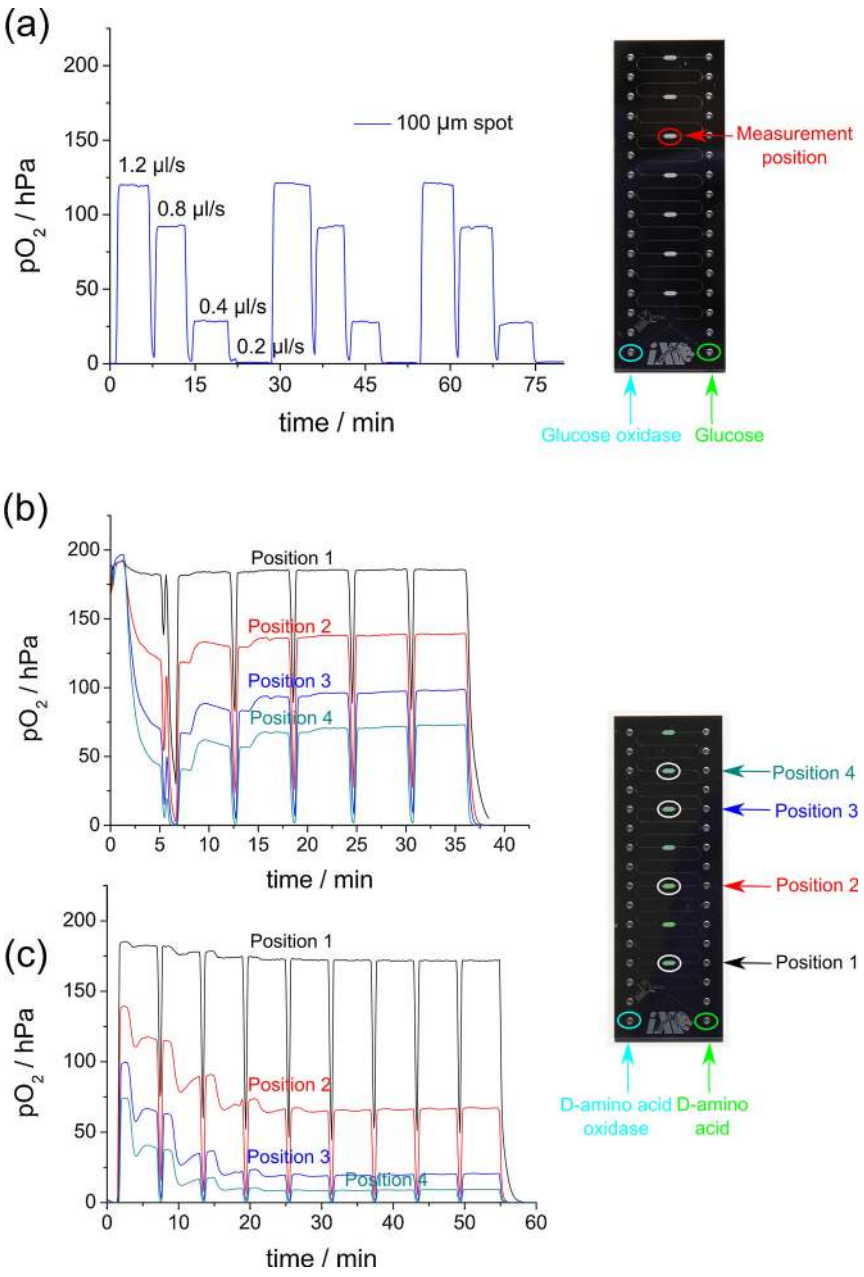

Fig. 6. Oxidation of glucose (a) to D-glucono-δ-lactone and hydrogen peroxide at flow rates of 1.2 μL/s, 0.8 μL/s, 0.4 μL/s and 0.2 μL/s were performed in *microreactor 1*. Oxidations of D-alanine (b) and D-phenylalanine (c) by D-amino acid oxidase at a flow rate of 0.6 μL/s were carried out in *microreactor 2*. All reactions were performed at room temperature.

oxygen by the enzyme. After approx. 8–15 min (depending on the measurement position) the system (pumps, tubes, solutions and microreactor) was stable and provided consistent oxygen concentrations. After 40 min D-alanine was replaced by D-phenylalanine [6(c)] and it required 20–25 min until the signal was stabilized again. This stabilization time of the microreactor is a function of the fluidic conditions (flow rate, channel geometry) and thus can be adjusted by changing these parameters. The oxygen concentrations for D-alanine and D-phenylalanine are shown in supplementary Table 1. As expected, D-phenylalanine is oxidized faster than D-alanine [40].

Microreactor 3 (channel dimensions: 400 μm deep, 200 μm wide, volume: 27.6 μL) did not contain sensing chambers and the oxygen sensor (PtTPTBPF) was directly integrated into the straight microfluidic structures with a width of 200 μm. Its response time (t_{90}) was about 3 s and determined by introducing gaseous nitrogen into the chip. Read out was performed by the 4-channel oxygen meter connected to optical fibres. An enzyme cascade reaction using glucose oxidase to deplete oxygen and catalase to reproduce oxygen was carried out in *microreactor 3* [Fig. 7(a)] and additionally in a modified version of *microreactor 2* [Fig. 7(b)] which contained PdTPTBPF and PtTPTBPF oxygen sensing layers. In detail the first three chambers of the modified version contained the PdTPTBPF sensors and the other four contained the PtTPTBPF sensors. The oxygen concentrations were simultaneously determined at four sensing areas (Fig. 7). Glucose and glucose oxidase were introduced separately over the two main inlets and catalase over a lateral inlet after the first two measurement areas. The third pump with catalase solution was switched on and off alternately (I and II in Fig. 7) to see the difference when the catalase is present/absent. It can be seen from Fig. 7 that the oxygen concentrations decrease from the first to the second measurement position. At the third position the oxygen

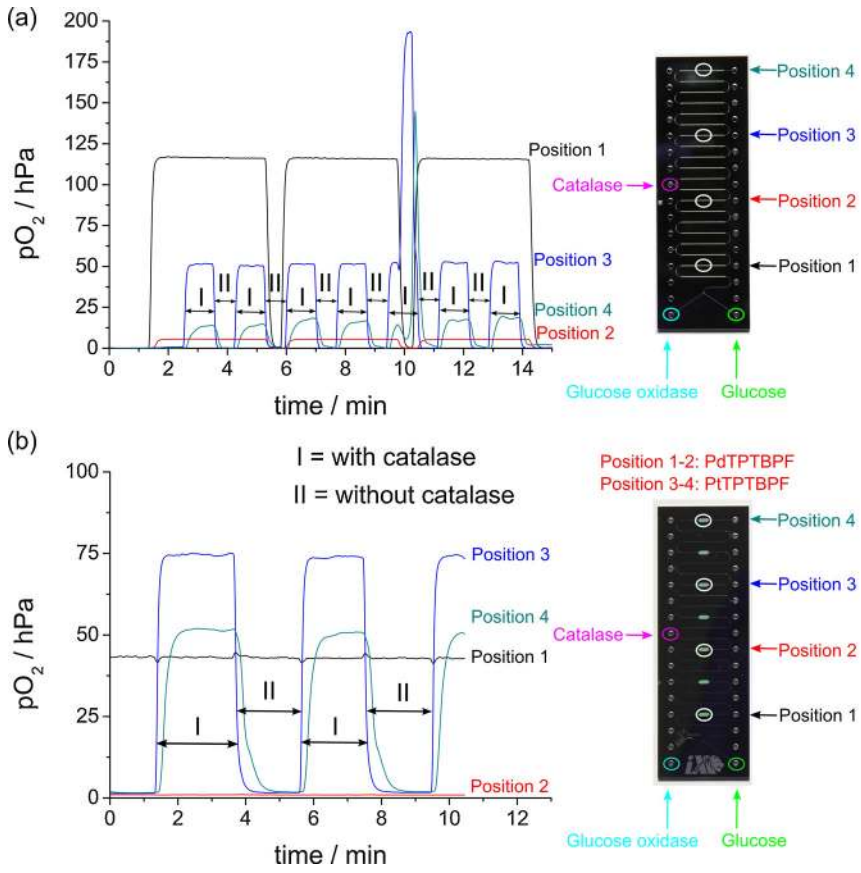

Fig. 7. Oxidation of glucose by glucose oxidase to D-glucono-δ-lactone and hydrogen peroxide, which was alternating reconverted into oxygen by adding catalase. Reactions were performed at room temperature in *microreactor 3* (a) and a modified version of *microreactor 2* (b). Pumps were operated at a flow rate of 0.1 μL/s.

concentration is increased when the third pump was switched on because of the introduction of air saturated catalase solution into the microreactor. At the fourth measurement position the oxygen levels are decreased again even when the third pump is switched on because the glucose oxidase is consuming the oxygen faster than the catalase can reproduce it. We indirectly tested the function of the catalase in another experiment by introducing just air saturated buffer over the lateral inlet and confirmed that the oxygen concentration at the third and fourth measurement position without catalase is significantly lower. The oxygen concentrations at different measurement positions are shown in Supplementary Table 2. As mentioned above the syringe pumps had to be refilled and therefore stopped pumping. The peak at approximately 10 min in Fig. 7(a) derived because catalase was introduced into the microreactor while the two other pumps stopped for refilling.

The enzyme reactions demonstrate that this measurement set-up is ideally suited for online monitoring of oxygen within microfluidic devices. The oxygen impermeability of the glass-silicon microreactor is beneficial compared to devices from PDMS or other polymeric materials because it avoids disturbing the oxygen intake from the surrounding chip material. Our microreactor system thus enables the investigation of oxygen depletion reactions within microfluidic devices and provides a useful tool for determining kinetic parameters at μ-scale in the future.

4. Conclusion

In summary, we report a powerful measurement-set up for microfluidic applications consisting of NIR-emitting optical oxygen sensors and an inexpensive and robust readout via commercially available oxygen meters adapted with gradient index lenses to enhance the signal intensities. The set-up enables the determination of oxygen up to a resolution of 0.06–0.22 hPa (approx. 3–9 μg/L of dissolved oxygen). Furthermore, the sensitivity of the sensor can be easily adjusted by the integration of different oxygen indicator dyes. Moreover, the integration and patterning of sensor layers into microreactors was demonstrated by automated airbrush spraying, a versatile method. Our fabricated microreactors consisted of silicon-glass composites, contained integrated oxygen sensor down to a size of 100 μm in diameter and were used to monitor enzyme reactions. In contrast to common polymeric chip materials, silicon and glass offer the advantage of being impermeable for oxygen and therefore the effect of the bulk material on the oxygen concentration is negligible. The microreactors can be used in future for kinetic studies of oxygen consuming or producing enzyme reactions, cell based respiration measurements or organ-on-chip applications.

Acknowledegments

Financial support by the European Union FP7 Project BIOINTENSE—Mastering Bioprocess integration and intensification across scales (Grant Agreement Number 312148) is gratefully acknowledged. Further we thank Dr. Tobias Abel for programming the syringe pumps and Assoc. Prof. Gregor Trimmel for the surface profile measurements.

Appendix A. Supplementary data

Supplementary data associated with this article can be found, in the online version, at http://dx.doi.org/10.1016/j.snb.2016.01.050.

References

[1] D.I. Paul Fletcher, S.J. Haswell, B.H. Pombo-Villar, P. Warrington, Y.F. Stephanie Wong, X. Zhang, Micro reactors: principles and applications in organic synthesis, Tetrahedron 58 (2002) 4735–4757.
[2] D.S. Peterson, T. Rohr, F. Svec, M.J. Fréchet Jean, Enzymatic microreactor-on-a-chip: protein mapping using trypsin immobilized on porous polymer monoliths molded in channels of microfluidic devices, Anal. Chem. 74 (2002) 4081–4088.
[3] G.H. Seong, J. Heo, R.M. Crooks, Measurement of enzyme kinetics using a continuous-flow microfluidic system, Anal. Chem. 75 (2003) 3161–3167.
[4] M.B. Kerby, R.S. Legge, A. Tripathi, Measurements of kinetic parameters in a microfluidic reactor, Anal.l Chem. 78 (2006) 8273–8280.
[5] L.T. Harry Lee, P. Boccazzi, R.J. Ram, A.J. Sinskey, Microbioreactor arrays with integrated mixers and fluid injectors for high-throughput experimentation with pH and dissolved oxygen control, Lab Chip 6 (2006) 1229–1235.
[6] G. Mehta, J. Lee, W. Cha, Y.-C. Tung, J.J. Linderman, S. Takayama, Hard top soft bottom microfluidic devices for cell culture and chemical analysis, Anal. Chem. 81 (2009) 3714–3722.
[7] H.W. Raymond Lam, M.-C. Kim, T. Thorsen, Culturing aerobic and anaerobic bacteria and mammalian cells with a microfluidic differential oxygenator, Anal. Chem. 81 (2009) 5918–5924.
[8] K.S. Lee, P. Boccazzi, A.J. Sinskey, R.J. Ram, Microfluidic chemostat and turbidostat with flow rate, oxygen, and temperature control for dynamic continuous culture, Lab Chip 11 (2011) 1730–1739.
[9] S.A. Pfeiffer, S. Nagl, Microfluidic platforms employing integrated fluorescent or luminescent chemical sensors: a review of methods, scope and applications, Methods Appl. Fluoresc. 3 (2015) 34003.
[10] S. Sun, B. Ungerböck, T. Mayr, Imaging of oxygen in microreactors and microfluidic systems, Methods Appl. Fluoresc. 3 (2015) 34002.
[11] S.M. Grist, L. Chrostowski, K.C. Cheung, Optical oxygen sensors for applications in microfluidic cell culture, Sensors (Basel) 10 (2010) 9286–9316.
[12] J.N. Demas, D. Diemente, E.W. Harris, Oxygen quenching of charge-transfer excited states of ruthenium(II) complexes. Evidence for singlet oxygen production, J. Am. Chem. Soc. 95 (1973) 6864–6865.
[13] C.J. Timpson, C.C. Carter, J. Olmsted, Mechanism of quenching of electronically excited ruthenium complexes by oxygen, J. Phys. Chem. 93 (1989) 4116–4120.
[14] Z.J. Fuller, W.D. Bare, K.A. Kneas, W.-Y. Xu, J.N. Demas, B.A. DeGraff, Photostability of luminescent ruthenium(II) complexes in polymers and in solution, Anal. Chem. 75 (2003) 2670–2677.
[15] B. Ungerböck, S. Fellinger, P. Sulzer, T. Abel, T. Mayr, Magnetic optical sensor particles: a flexible analytical tool for microfluidic devices, Analyst 139 (2014) 2551–2559.
[16] A. Sin, K.C. Chin, M.F. Jamil, Y. Kostov, G. Rao, M.L. Shuler, The design and fabrication of three-chamber microscale cell culture analog devices with integrated dissolved oxygen sensors, Biotechnol. Prog. 20 (2004) 338–345.
[17] A.P. Vollmer, R.F. Probstein, R. Gilbert, T. Thorsen, Development of an integrated microfluidic platform for dynamic oxygen sensing and delivery in a flowing medium, Lab Chip 5 (2005) 1059–1066.
[18] Raymond H.W. Lam, M.-C. Kim, T. Thorsen, Culturing aerobic and anaerobic bacteria and mammalian cells with a microfluidic differential oxygenator, Anal. Chem. 81 (2009) 5918–5924.
[19] V. Nock, R.J. Blaikie, T. David, Patterning, integration and characterisation of polymer optical oxygen sensors for microfluidic devices, Lab Chip 8 (2008) 1300–1307.
[20] V. Nock, M. Alkaisi, R.J. Blaikie, Photolithographic patterning of polymer-encapsulated optical oxygen sensors, Microelectron. Eng. 87 (2010) 814–816.
[21] J.R. Etzkorn, W.-C. Wu, Z. Tian, P. Kim, S.-H. Jang, D.R. Meldrum, A.K.-Y. Jen, B.A. Parviz, Using micro-patterned sensors and cell self-assembly for measuring the oxygen consumption rate of single cells, J. Micromech. Microeng. 20 (2010) 95017.
[22] T.W. Molter, S.C. McQuaide, M.T. Suchorolski, T.J. Strovas, L.W. Burgess, D.R. Meldrum, M.E. Lidstrom, A microwell array device capable of measuring single-cell oxygen consumption rates, Sens. Actuators B Chem. 135 (2009) 678–686.
[23] A. Zanzotto, N. Szita, P. Boccazzi, P. Lessard, A.J. Sinskey, K.F. Jensen, Membrane-aerated microbioreactor for high-throughput bioprocessing, Biotechnol. Bioeng. 87 (2004) 243–254.
[24] N. Szita, P. Boccazzi, Z. Zhang, P. Boyle, A.J. Sinskey, K.F. Jensen, Development of a multiplexed microbioreactor system for high-throughput bioprocessing, Lab Chip 5 (2005) 819–826.
[25] A. Zanzotto, P. Boccazzi, N. Gorret, A.J. Van Dyk, K.F. Jensen, In situ measurement of bioluminescence and fluorescence in an integrated microbioreactor, Biotechnol. Bioeng. 93 (2006) 40–47.
[26] P.C. Thomas, M. Halter, A. Tona, S.R. Raghavan, A.L. Plant, S.P. Forry, A noninvasive thin film sensor for monitoring oxygen tension during in vitro cell culture, Anal. Chem. 81 (2009) 9239–9246.
[27] P.C. Thomas, S.R. Raghavan, S.P. Forry, Regulating oxygen levels in a microfluidic device, Anal. Chem. 83 (2011) 8821–8824.
[28] B. Ungerbock, V. Charwat, P. Ertl, T. Mayr, Microfluidic oxygen imaging using integrated optical sensor layers and a color camera, Lab Chip 13 (2013) 1593–1601.
[29] L. Gitlin, C. Hoera, R.J. Meier, S. Nagl, D. Belder, Micro flow reactor chips with integrated luminescent chemosensors for spatially resolved on-line chemical reaction monitoring, Lab Chip 13 (2013) 4134–4141.
[30] S.M. Grist, N. Oyunerdene, J. Flueckiger, J. Kim, P.C. Wong, L. Chrostowski, K.C. Cheung, Fabrication and laser patterning of polystyrene optical oxygen sensor films for lab-on-a-chip applications, Analyst 139 (2014) 5718–5727.
[31] L.C. Lasave, S.M. Borisov, J. Ehgartner, T. Mayr, Quick and simple integration of optical oxygen sensors into glass-based microfluidic devices, RSC Adv. 5 (2015) 70808–70816.
[32] G.A. Thete, T. Gross, Microfluidic arrangement with an integrated micro-spot array for the characterization of pH and solvent polarity, Microreaction Technology IMRET 9: Proceedings of the Ninth International Conference on Microreaction Technology IMRET9 Special Issue 135, Supplement 1 (2008) S327–S332.
[33] A.R. Thete, G.A. Gross, J.M. Koehler, Differentiation of liquid analytes in gel films by permeability-modulated double-layer chemo-chips, Analyst 134 (2009) 394–400.
[34] C. Herzog, E. Beckert, S. Nagl, Rapid isoelectric point determination in a miniaturized preparative separation using jet-dispensed optical pH sensors and micro free-flow electrophoresis, Anal. Chem. 86 (2014) 9533–9539.
[35] E. Poehler, C. Herzog, M. Suendermann, S.A. Pfeiffer, S. Nagl, Development of microscopic time-domain dual lifetime referencing luminescence detection for pH monitoring in microfluidic free-flow isoelectric focusing, Eng. Life Sci. 15 (2015) 276–285.
[36] S.M. Borisov, G. Nuss, I. Klimant, Red light-excitable oxygen sensing materials based on platinum(II) and palladium(II) benzoporphyrins, Anal. Chem. 80 (2008) 9435–9442.
[37] S.M. Borisov, G. Zenkl, I. Klimant, Phosphorescent platinum(II) and palladium(II) complexes with azatetrabenzoporphyrins—new red laser diode-compatible indicators for optical oxygen sensing, ACS Appl. Mater. Interfaces 2 (2010) 366–374.
[38] B.J. Müller, T. Burger, S.M. Borisov, I. Klimant, High performance optical trace oxygen sensors based on NIR-emitting benzoporphyrins covalently coupled to silicone matrixes, Sens. Actuators B: Chem. 216 (2015) 527–534.
[39] J.N. Demas, B.A. DeGraff, W. Xu, Modeling of luminescence quenching-based sensors: comparison of multisite and nonlinear gas solubility models, Anal. Chem. 67 (1995) 1377–1380.
[40] A. D'Aniello, A. Vetere, L. Petrucelli, Further study on the specificity of D-amino acid oxidase and of D-aspartate oxidase and time course for complete oxidation of D-amino acids, Comp. Biochem. Physiol. Part B: Comp. Biochem. 105 (1993) 731–734.

Biographies

Josef Ehgartner is currently a Ph.D. student at the Institute of Analytical Chemistry and Food Chemistry at the Graz University of Technology. In 2013 he received his master's degree in chemistry pursuing the analysis of arsenolipids in algae. His research interests revolve around the development of analytical methods, especially the development of optical sensors and their use in microfluidic devices.

Philipp Sulzer is studying Technical Chemistry at the Graz University of Technology. He is currently working on his master thesis at the Institute of Analytical Chemistry and Food Chemistry. His work consists of the application and improvement of different preparation methods for optical sensor layers, especially microdispensing technology.

Tobias Burger is currently doing his Masters in chemistry at the Zurich University of Applied Sciences. He was working at the Institute of Analytical Chemistry and Food Chemistry on the synthesis of different indicators for optical oxygen sensors.

Alice Kasjanow, holds a Master of Engineering, graduated at the University of Applied Science, Kaiserslautern/Zweibrücken. After her graduation she joined iX-factory as process engineer. Her present specialisation lies in MEMS processing of silicon and glass, and bonding technologies.

Dominique Bouwes. Dominique Bouwes holds a Diploma (Dipl.-Ing. FH) and a Master in Engineering from Kaiserslautern University of Applied Sciences site Zweibrücken, Germany, with the specialisation Micro Systems Technology (2002, 2006). During her studies she worked as Scientific Assistant at the Fraunhofer Institute for Biomedical Engineering St. Ingbert epartment sensor systems/micro systems and at the University of Twente, MESA+, Institute of Nanotechnology, Enschede, The Netherlands. After her graduation Dominique Bouwes joined the University of Twente, Enschede in The Netherlands as Process and Research Engineer. Since 2007 she is CEO and shareholder of the company. Dominique Bouwes is specialised in Micro-and Nanotechnologies silicon etching and stamp fabrication.

Ulrich Krühne is currently Associate Professor at the Department of Chemical and Biochemical Engineering at the Technical University of Denmark. He has obtained his Ph.D. at the same department in Denmark. He graduated as M.Sc. at the Technical University of Belin in Germany. After his Ph.D. he has worked for 3 years in a Danish start up company (Celtor Biosystems A/S) and 8 years in a private research institute (Danish Technological Institute). His Research interests include process intensification, micro-technology and microfluidics as well as computational fluid dynamics applied to chemical and biochemical applied research.

Ingo Klimant received his Ph.D. in chemistry in 1993 from the Karl-Franzens University in Graz. Since 2001 he is full professor at the Institute of Analytical Chemistry and Food Chemistry of the Graz University of Technology (Austria). His areas of interest include optical chemical sensors, analytical methods in biotechnology and molecule spectroscopy

Torsten Mayr received his Ph.D. in chemistry from the University of Regensburg (Germany) in 2004. In 2002–2004 he was a post-doctoral fellow at the Karolinska Institute in Stockholm (Sweden). Since 2004 he is assistant professor at the Institute of Analytical Chemistry and Food Chemistry at the Graz University of Technology. Since 2014 he is Associate Professor the same institute. His research interests include optical chemical sensors, biosensors, functionalized micro- and nanoparticles and microfluidic systems.